IN-20-CR
61517
P 25

FINAL REPORT

LOW THRUST VISCOUS NOZZLE FLOW FIELDS PREDICTION

GRANT NAG8-064
1986-1991

SUBMITTED TO

NATIONAL AERONAUTICS AND SPACE ADMINISTRATION
MARSHALL SPACE FLIGHT CENTER

BY
G. S. LIAW and J. D. MO

SCHOOL OF ENGINEERING AND TECHNOLOGY
ALABAMA AGRICULTURAL AND MECHANICAL UNIVERSITY
NORMAL, AL 35762

DECEMBER, 1991

Forward

This document presents the results of the research work performed by Drs. G. S. Liaw and J. D. Mo of Alabama A&M university for NASA/Marshall Space Flight Center, under Grant NAG8-064. Two major tasks were accomplished during the course of this research project. First, a new computer code was developed for the low thrust viscous nozzle flowfield predictions by using a new LU scheme. This task was proposed at the beginning of this contract. Second, the existing FDNS code was implemented to include the radiation effect. This task was added into this project later. Results for a Carbon Dioxide and the SSME nozzles are documented in this final report.

Table of Contents

I. Introduction

This research project has three objectives. The first objective is to compute the Carbon Dioxide nozzle flow fields by using an existing computer code. This work has been completed and documented previously[1]. The second objective is to develop a new computer code for solving the compressible full Navier-Stokes equations for low thrust type nozzle flow calculations. The low density effect is embedded through the no-slip conditions on the wall boundaries. The third objective is to analyze the space shuttle Main Engine (SSME) flow field in the combustor and the divergent nozzle with radiative effect. The radiation model has been derived and embedded into the existing FDNS computer code which is currently operational in ED32 NASA/MSFC. However, our main contribution is to develop a compressible Navier-Stokes code which is capable of handling the rarefication effect.

Basically, there are two kind of numerical schemes to solve the time-dependent fluid dynamics problems. They are explicit or implicit. The early developments, limited by the computer capability, emphasized on the explicit methods. Several explicit numerical schemes have been developed successfully, such as the Euler explicit method, the Lax method, Leap frog method, MacCormack method, etc.. The obvious way to accelerate convergence to a steady state or to save the computer time for unsteady problems is to increase the size of the time step. However, it was found that the time step size for the explicit schemes is seriously limited by the Courant-Friedrichs-Lewy (CFL) condition, which requires that the region of dependence of the difference scheme must be a subset of the region of dependence of the differential equation.

Generally speaking, implicit schemes are preferred when the time step limit imposed by an explicit bound is much less than that imposed by the accuracy bound. The computation is unconditionally stable for implicit schemes, and the time step is determined by the desired level of accuracy. However, the implicit methods require to solve a large number of coupled equations at each time step. Hence, the reduction in the number of time steps may be outweighed by the increase in the number of arithmetic operations required for each time step. As the computer technology advances, the restrictions on the storage and computing time have been relaxed. The implicit methods become more popular in the CFD community.

In this work, a Navier-Stokes code has been developed for the low thrust viscous nozzle flow fields prediction. An implicit finite volume, in an arbitrary curvilinear coordinate system, lower-upper(LU) scheme[2] is used to solve the governing Navier-Stokes equations and species transportation equations. This scheme was originally developed by Jameson, and extended to an axisymmetric coordinate system by this group. Sample calculations of Carbon Dioxide nozzle flow are presented in this report to verify the validity and efficiency of this code. The computed results are in reasonable agreement with the experimental data. The bench mark date were chosen from Chou and Carter[3].

II. The LU-Code Development

2.1. Formulation

Basic governing equations: The governing Navier-Stokes equations are derived from the basic physical laws of conservation of mass, momentum and energy. These equations are cast into the conservative forms in the cylindrical coordinate system

$$\frac{\partial Q}{\partial t}+\frac{\partial (F-F_v)}{\partial x}+\frac{\partial (G-G_v)}{\partial y}=S \tag{2.1}$$

where

$$Q=\begin{bmatrix}\rho\\ \rho u\\ \rho v\\ \rho E\\ \rho Y_i\end{bmatrix}$$

$$F=\begin{bmatrix}\rho u\\ \rho u^2+p\\ \rho u v\\ u(\rho E+p)\\ \rho u Y_i\end{bmatrix}, \qquad F_v=\begin{bmatrix}0\\ \tau_{xx}\\ \tau_{xy}\\ u\tau_{xx}+v\tau_{xy}-q_x\\ -\rho \tilde{u}_j Y_i\end{bmatrix}$$

$$G=\begin{bmatrix}\rho v\\ \rho u v\\ \rho v^2+p\\ v(\rho E+p)\\ \rho v Y_i\end{bmatrix}, \qquad G_v=\begin{bmatrix}0\\ \tau_{xy}\\ \tau_{yy}\\ u\tau_{xy}+v\tau_{yy}-q_y\\ -\rho \tilde{v}_j Y_i\end{bmatrix}$$

$$S=S_1+S_2+S_3=\begin{bmatrix}0\\ 0\\ 0\\ 0\\ w_j\end{bmatrix}+\frac{\delta}{r}\begin{bmatrix}-\rho v\\ -\rho u v\\ -\rho v^2\\ -v(\rho E+p)\\ -\rho v Y_i\end{bmatrix}+\frac{\delta}{r}\begin{bmatrix}0\\ \tau_{xy}\\ \tau_{yy}\\ u\tau_{xy}+v\tau_{yy}-q_y\\ -\rho \tilde{v}_i Y_i\end{bmatrix}$$

This set of compressible flow equations govern the steady or unsteady; laminar or turbulent, chemically reacting or nonreacting flow problems. S is the summation of all the source terms, while δ=0 for the rectangular coordinate and δ=1 for the axisymmetric coordinate system.

Grid generation and coordinate transformation: The numerical solution of the system of the governing partial differential equations can be greatly simplified by a well constructed grid network. It is also true that a grid which is not well suited to the problem can produce unsatisfactory results. Improper choice of grid point locations may lead to an apparent instability.

Early numerical solution by finite difference methods was restricted to problems where suitable coordinate systems must be selected in order to solve the governing equations in this compatible coordinate system. As more complex flowfields problems are under consideration, general mappings have been employed to transform the physical plane into a computational domain. Numerous advantages accrue when appropriate transfer procedures are followed, for example, the body surface can be selected as a boundary in the computational plane permitting easy application of surface boundary conditions. Also, in general, transformation is used which lead to a uniformly spaced grid in the computational plane while points in physical space may be unequally spaced.

For general purposes, consider the following general transformation, which can be orthogonal or nonorthogonal,

$$\xi = \xi(x,y) \tag{2.2}$$

$$\eta = \eta(x,y) \tag{2.3}$$

the computational grid points are located along the transformed coordinates (ξ, η), which can be designed to have both equal or unequal spacing in the computational plane depending on the problems.

Generally, the grid generation can be accomplished by three different approaches.

* the complex variable method,
* the algebraic method and
* the differential equations method.

The complex variable technique has the advantage that the transformations used are analytic or partially analytic as opposed to those methods that are entirely numerical. Unfortunately, complex variable methods are restricted in two dimensional problem. For this reason, the technique has limited applicability and will not be used in the present work. Algebraic and differential equation techniques can be used on both two and three dimensional problems with complex geometry, they are adopted in this code development.

To be consistent with the general grid system, a corresponding coordinate transformation on the governing partial differential equation is required. The requirements of this transformation for grid generation are:

* The mapping is one - one correspondent, i.e. no singularity exists in the mapping function.
* The grid lines is smooth to assure that the derivatives of the mapping function are continuous.
* Grid points are closely clustered in the region where the large numerical errors are expected.
* Avoid excessive grid skewness.

For the transformation (2.2) and (2.3), the governing equations are converted from the

physical domain (x, y) to the computational domain (ξ, η). By using the chain rule of partial differentiation, the partial derivative becomes

$$\frac{\partial}{\partial x} = \xi_x \frac{\partial}{\partial \xi} + \eta_x \frac{\partial}{\partial \eta} \tag{2.4}$$

$$\frac{\partial}{\partial y} = \xi_y \frac{\partial}{\partial \xi} + \eta_y \frac{\partial}{\partial \eta} \tag{2.5}$$

The matrices (ξ_x, ξ_y, η_x, η_y) appearing in these equations can be determined in the following manner:

$$d\xi = \xi_x dx + \xi_y dy \tag{2.6}$$

$$d\eta = \eta_x dx + \eta_y dy \tag{2.7}$$

or in the matrix form

$$\begin{bmatrix} d\xi \\ d\eta \end{bmatrix} = \begin{bmatrix} \xi_x & \xi_y \\ \eta_x & \eta_y \end{bmatrix} \begin{bmatrix} dx \\ dy \end{bmatrix} \tag{2.8}$$

In a similar manner, we can write

$$\begin{bmatrix} dx \\ dy \end{bmatrix} = \begin{bmatrix} x_\xi & x_\eta \\ y_\xi & y_\eta \end{bmatrix} \begin{bmatrix} d\xi \\ d\eta \end{bmatrix} \tag{2.9}$$

therefore:

$$\begin{bmatrix} \xi_X & \xi_Y \\ \eta_X & \eta_Y \end{bmatrix} = \begin{bmatrix} X_\xi & X_\eta \\ Y_\xi & Y_\eta \end{bmatrix}^{-1} = \frac{1}{J} \begin{bmatrix} Y_\eta & -X_\eta \\ -Y_\xi & X_\xi \end{bmatrix} \tag{2.10}$$

where the Jacobian

$$J = \left| \frac{\partial(\xi, \eta)}{\partial(X, Y)} \right| = \begin{vmatrix} \xi_X & \xi_Y \\ \eta_X & \eta_Y \end{vmatrix} = \frac{1}{J^{-1}} = \frac{1}{\left| \frac{\partial(X, Y)}{\partial(\xi, \eta)} \right|} = \frac{1}{X_\xi Y_\eta - X_\eta Y_\xi} \tag{2.11}$$

The terms x_ξ, x_η , y_ξ, and y_η are obtained directly by the central difference. Then, the quantities ξ_x, ξ_y, η_x, η_y, which appear in the governing equation, are evaluated from equation (2.10).

$$\xi_x = \frac{Y_\eta}{J} = \frac{1}{J}\frac{Y_{i,j+1} - Y_{i,j-1}}{2\,\Delta\eta_{i,j}}$$

$$\xi_Y = -\frac{X_\eta}{J} = -\frac{1}{J}\frac{X_{i,j+1} - X_{i,j-1}}{2\,\Delta\eta_{i,j}}$$

$$\eta_x = -\frac{Y_\xi}{J} = -\frac{1}{J}\frac{Y_{i+1,j} - Y_{i-1,j}}{2\,\Delta\xi_{i,j}}$$

$$\eta_Y = \frac{X_\xi}{J} = \frac{1}{J}\frac{X_{i+1,j} - X_{i-1,j}}{2\,\Delta\xi_{i,j}}$$

After the coordinate transformation, the governing equation (2.1) becomes:

$$\frac{\partial Q}{\partial t} + \xi_x \frac{\partial (F - F_v)}{\partial \xi} + \eta_x \frac{\partial (F - F_v)}{\partial \eta} + \xi_y \frac{\partial (G - G_v)}{\partial \xi} + \eta_y \frac{\partial (G - G_v)}{\partial \eta} = S$$

The strong conservation form of the above equations are

$$\frac{\partial Q}{\partial t} + \frac{\partial}{\partial \xi}\left[\xi_x (F - F_v) + \xi_y (G - G_v)\right] + \frac{\partial}{\partial \eta}\left[\eta_x (F - F_v) + \eta_y (G - G_v)\right] = S$$

It can be written in a compact form,

$$\frac{\partial Q}{\partial t} + \frac{\partial (f - f_v)}{\partial \xi} + \frac{\partial (g - g_v)}{\partial \eta} = S \qquad (2.12)$$

where

$$f = \xi_x F + \xi_y G, \qquad f_v = \xi_x F_v + \xi_y G_v$$

$$g = \eta_x F + \eta_y G, \qquad f_v = \eta_x F_v + \eta_y G_v$$

and S the source term is unchanged by the transformation.

2.2. Numerical Procedures

Linearization of the governing equations by the delta form formulation: For simplicity, the derivation of the equations below is carried out in the Cartesian coordinate system, then the results are transformed onto a general coordinate system.

Using the implicit scheme with central differencing, Eq. (2.12) can be formulated as

$$Q^{n+1} = Q^n - \beta \delta t \left\{ \partial_\xi \left(f(Q^{n+1}) - f_v(Q^{n+1}) \right) + \partial_\eta \left(g(Q^{n+1}) - g_v(Q^{n+1}) \right) - S^{n+1} \right\}$$
$$-(1-\beta)\delta t \left\{ \partial_\xi \left(f(Q^n) - f_v(Q^n) \right) + \partial_\eta \left(g(Q^n) - g_v(Q^n) \right) - S^n \right\} \qquad (2.13)$$

where $\partial\xi$ and $\partial\eta$ are difference operators of $\partial/\partial\xi$, $\partial/\partial\eta$, and β is a positive number between 0 and 1, which is used as an adjust parameter, with $\beta=0$ for an explicit scheme and $\beta=1$ for an implicit scheme. $\beta=1/2$ is designated for the Crank-Nicolson scheme which has a second order accuracy in the time discretization.
The Jacobian matrices are

$$A = \frac{\partial (F - F_v)}{\partial Q} \qquad B = \frac{\partial (G - G_v)}{\partial Q} \qquad \text{and} \qquad H = \frac{\partial S}{\partial Q} \qquad (2.14)$$

and the increment of the conservative variable Q is

$$\delta Q = Q^{n+1} - Q^n \qquad (2.15)$$

The scheme is linearized by setting

$$f(Q^{n+1}) = f(Q^n) + \frac{\partial f}{\partial Q} \delta Q + O(|\delta Q|^2)$$

$$g(Q^{n+1}) = g(Q^n) + \frac{\partial g}{\partial Q} \delta Q + O(|\delta Q|^2)$$

$$S(Q^{n+1}) = S(Q^n) + \frac{\partial S}{\partial Q} \delta Q + O(|\delta Q|^2) \qquad (2.16)$$

where terms of the second and higher order have been omitted. This yields,

$$Q^{n+1} - Q^n = -\beta \Delta t \left\{ \partial_\xi \left(f(Q^n) - f_v(Q^n) \right) + \partial_\xi AA\, \delta Q \right\}$$
$$-\beta \Delta t \left\{ \partial_\eta \left(g(Q^n) - g_v(Q^n) \right) + \partial_\eta BB \delta Q \right\}$$
$$-\beta \Delta t \left\{ -S^n - H \delta Q \right\}$$
$$-(1-\beta)\Delta t \left\{ \partial_\xi \left(f(Q^n) - f_v(Q^n) \right) + \partial_\eta \left(g(Q^n) - g_v(Q^n) \right) - S^n \right\} \qquad (2.17)$$

In compact form, the final δ-form of equation (2.17) becomes

$$\left\{ I + \beta\, \Delta t \left(\partial_\xi AA + \partial_\eta BB - H \right) \right\} + \Delta t\, R = 0 \qquad (2.18)$$

where

$$AA = \frac{\partial (f - f_v)}{\partial Q} = \xi_x A + \xi_y B \tag{2.19}$$

$$BB = \frac{\partial (g - g_v)}{\partial Q} = \eta_x A + \eta_y B \tag{2.20}$$

$$HH = \frac{\partial S}{\partial Q} = H \tag{2.21}$$

and

$$R = \left\{ \partial_\xi (f - f_v) + \partial_\eta (g - g_v) \right\} - S^n \tag{2.22}$$

Lower-Upper (LU) factored implicit scheme: There are various ways to formulate an LU scheme. We begin with the following procedures, by setting,

$$\partial\xi = (\partial\xi^+ + \partial\xi^-) \tag{2.23}$$

$$\partial\eta = (\partial\eta^+ + \partial\eta^-) \tag{2.24}$$

with the definitions of matrices

$$AA^+ = 1/2\,(AA + \nu_A I) \tag{2.25}$$

$$AA^- = 1/2\,(AA - \nu_A I) \tag{2.26}$$

then

$$\partial\xi\, AA = \partial\xi^+ AA^- + \partial\xi^- AA^+ \tag{2.27}$$

In the similar manner,

$$\partial\eta\, AA = \partial\eta^+ BB^- + \partial\eta^- BB^+ \tag{2.28}$$

where,

$$BB^+ = 1/2\,(BB + \nu_B I) \tag{2.29}$$

$$BB^- = 1/2\,(BB - \nu_B I) \tag{2.30}$$

After substitution, equation (3.7) becomes

$$\left\{ I + \beta\, \Delta t \left(\partial_\xi^- AA^+ + \partial_\xi^+ AA^- + \partial_\eta^- BB^+ + \partial_\eta^+ BB^- - H \right) \right\} \delta Q = -\Delta t R \tag{2.31}$$

where $\partial\xi^-$ and $\partial\eta^-$ are defined as backward-difference operators and $\partial\xi^+$ and $\partial\eta^+$ are defined as forward difference operators.

The values ν_A and ν_B are chosen to construct AA^+, AA^-, BB^+, BB^- so that the eigenvalues of "+" matrices are nonnegative and those of "-" matrices are nonpositive. The development of these matrices is extremely important for the success of the LU-type scheme.

Jameson and Yoon [4] chose

$$\nu_A \geq \max\left(|\lambda_A| \right) \tag{2.32}$$

$$\nu_B \geq \max\left(|\lambda_B| \right) \tag{2.33}$$

where λ_A and λ_B are the eigenvalues of matrix AA and BB.

After some manipulations, equation (2.31) becomes:

$$\left\{ I + \beta \Delta \left[(AA^{+} - AA^{-}) + (BB^{+} - BB^{-}) \right] + \beta \Delta t \left(\partial_{\xi}^{-} AA^{+} + \partial_{\xi}^{+} AA^{-} + \partial_{\eta}^{-} BB^{+} + \partial_{\eta}^{+} BB^{-} - (AA^{+} - AA^{-}) - (BB^{+} - BB^{-}) - H \right) \right\} \delta Q$$

$$= -\Delta t R \tag{2.34}$$

From (2.25), (2.26), (2.29) and (2.30),

$$AA^{+} - AA^{-} = \nu_A I$$

$$BB^{+} - BB^{-} = \nu_B I$$

Equation (2.34) can be factored in the following forms

$$\left\{ I + \beta \Delta t \left[(AA^{+} - AA^{-}) + (BB^{+} - BB^{-}) \right] + \beta \Delta t \left(\partial_{\xi}^{-} AA^{+} + \partial_{\eta}^{-} BB^{+} - AA^{+} - BB^{+} - H \right) \right\}$$

$$* \left\{ I + \beta \Delta t \left[(AA^{+} - AA^{-}) + (BB^{+} - BB^{-}) \right] + \beta \Delta t \left(\partial_{\xi}^{+} AA^{-} + \partial_{\eta}^{+} BB^{-} + AA^{-} + BB^{-} \right) \right\} \delta Q$$

$$= -\left[1 + \beta \Delta t (\upsilon_A + \upsilon_B) \right] \Delta t R \tag{2.35}$$

This factorization is arbitrary as long as the final numerical scheme is stable. On the other hand, a further improvement on the scheme can be done from this point.

Numerical discretization and computational procedures: Based on the discretized governing equation (2.35), a finite-volume method is applied to discrete the spatial variable and separated time and spatial discretization is involved to assure a steady state solution independent of the time step. The finite volume formulation provides a convenient treatment of complex geometry and avoids the problems of metric singularity which are usually associated with the finite difference methods.

The control volume is shown in the Fig. 1. Point P is chosen as the control point located at the centroid of the control volume.

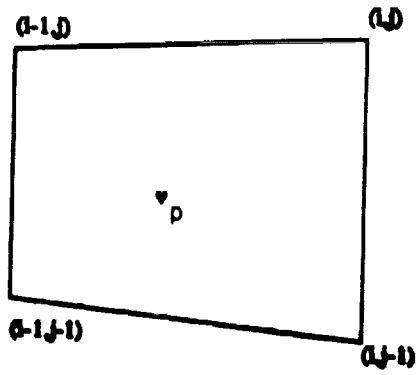

Fig. 1. Control volume and control point

By integrating the equation (2.35) over the control volume, the left hand side of the equation take the value at the control point as its average value. The first two terms in the right hand side constitute a divergent vectors and they are envoluated by a surface integration after applying the Gauss theorem. The residual source term takes the value at the control point.

In order to match the approximated factorization of the lower-upper triangular matrix form, the derivatives in the left hand side is discretized by the first order backward and forward difference schemes, such that

$$\partial_\xi^- Q^n = \frac{Q^n_{i,j} - Q^n_{i-1,j}}{\Delta\xi^-}, \qquad \partial_\xi^+ Q^n = \frac{Q^n_{i+1,j} - Q^n_{i,j}}{\Delta\xi^+} \tag{2.36}$$

$$\partial_\eta^- Q^n = \frac{Q^n_{i,j} - Q^n_{i,j-1}}{\Delta\eta^-}, \qquad \partial_\eta^+ Q^n = \frac{Q^n_{i,j+1} - Q^n_{i,j}}{\Delta\eta^+} \tag{2.37}$$

where the subscripts (i,j) represent the location of the grid point (ξ,η) and superscript stands for the time level, in which superscript n means at the time t and n+1 means at time $t+\Delta t$. $\Delta\xi^-$ is the projected spatial distance between the control point (i-1,j) and (i,j) in ξ coordinate direction and $\Delta\eta$ is the projected spatial distance between the control point (i,j-1) and (i,j) in η coordinate direction. $\Delta\xi^+$ and $\Delta\eta^+$ are similarly defined.

After the discretization of the partial differential equations, they become a system of algebraic equations. The continuous governing partial differential equations have been replaced by a set of discretized finite difference equations which are valid only at the discretized grid points. At each grid point, a finite difference equation is created and the connection among all the grid points in the solution domain is hold by the forward and backward finite difference operators. With proper boundary conditions at the boundaries of the solution domain and initial conditions at the beginning of the physical process for the unsteady problems, the set of the algebraic equations can be solved by proper numerical procedures.

A mathematical problem is described by the following algebraic equations to illustrate the essence of the lower-upper factorization procedures of the matrix conversion.

$$A\,X = b \tag{2.38}$$

If the coefficient matrix A can be decomposed into a lower-upper matrix multiplication

form, then the equation (2.38) can be rewritten as

$$LU\,X = b \tag{2.39}$$

Then we can solve this equation in two steps. At first, let Y=U X, equation (3.31) becomes

$$L\,Y = b \tag{2.40}$$

Because the matrix L is a lower triangular matrix, Its inverse L^{-1} can be easily determined by the forward Gaussian elimination method, or

$$Y = L^{-1}\,b \tag{2.41}$$

Then, looking for the solution for x such that

$$U\,X = Y \tag{2.42}$$

Since U is an upper triangular matrix, the matrix inverse can be found by the one step backward Gaussian elimination method,

$$X = U^{-1}\,Y \tag{2.43}$$

The lower-upper factorization procedure in the present research follows the same procedures as described above. The dimension of the final coefficient matrix is

$$[\,C\,] = [\,(I \times J) \times (I \times J)\,]$$

where I and J are the grid number in the ξ and η directions respectively.

Boundary conditions: Two types of geometrical boundaries are considered. One is solid walls, the other is non-solid walls which includes inlets, the symmetric axis, and planes of symmetry.

Solid walls: The no-slip conditions are applied on any solid walls, . In addition, zero pressure gradient are employed.

Inlet: For generality, any part of the boundaries is referred as inlet where the flow is inward to the solution domain. At the inlet, the flow variables are assumed known. That is, the velocities, static pressure and temperature are specified.

Exit: In the same way, any part of the boundary is classified as exit where the flow is outward to the solution domain. For generality, the exit is divided into two categories, which are supersonic or subsonic exits. For supersonic exits, no boundary conditions are needed because its hyperbolic nature. For subsonic exits, back pressure must be specified, and other flow variables apply

$$\frac{\partial^2 \phi}{\partial \xi^2} = 0 \tag{2.44}$$

where ϕ represents any flow variable except the static pressure.

It should be noted that even for supersonic exit, a boundary layer exists near the exit wall. So a known backpressure is applied in the subsonic boundary layer region.

Initial condition: Our interest is to achieve steady state solutions even though the procedures described above are valid for general unsteady flow problems.Therefore, only an appropriate initial solution is needed to start the time-iterative scheme, and finally the steady state solution is reached through the time marching process. For nozzle flows, an one dimensional inviscid supersonic solution is used as the initial condition.

2.3. Computer Program

The computer program has been structured in a general manner. At the present state, the program can treat compressible flows, turbulent as well as lamilar, chemically reactive as well as non-reactive, internal as well as external, two-dimensional or axisymmetric arbitrary geometry problems. Variable transport properties are also included.

The program structure is written in a modular form so that subroutines for specific physical effects can be flagged only when those effects are needed. After its execution, the main processor writes a considerable amount of information to external data files. This information is used by the postprocessor to produce a variety of computer graphic displays. These data will be made use of to restart the calculations in the future work. Most physical and numerical control parameters can be changed which gives the users considerable flexibility for their specific purposes. the basic flow diagram of the computer program is shown in Fig. 2.

2.4. Carbon Dioxide Nozzle Flow Calculation

For nozzle flowfield calculations, five reservoir pressures (29.4, 14.7, 7.35, 3.7,1.85)psi were run and shown in Fig.3. The reservoir temperature is fixed at 600^{O}F. Due to the cryogenic flow conditions in downstream, all the variable transport properties including the specific heat ratio are curve-fitted and extrapolated to extremely low temperature, shown in Fig.4. As for the boundary layer development at different chamber pressures, the velocity profiles and the boundary thicknesses at the nozzle exit are shown in Fig.5(a) and 5(b), respectively. The boundary layer thicknesses is defined at the boundary edge where the velocity magnitude is 99% of the core flow. It is found that the lower the chamber pressure, the thicker the boundary layer at the nozzle exit. This flow characteristics is due to the Reynolds number resulted from the low chamber pressure.For the chamber pressure 1.85psi, the boundary layer thickness is about one third of nozzle exit radius. As a result, the conventional MOC/BL concept is no longer applicable. The wall pressures of both computed and test data are shown in Fig.6. Fig.6(a) and 6(b) show the wall pressure distributions in linear and logarithmic scales. They are in good agreement. Test data asymptotically deteriorate as the exit pressures and temperatures approach the liquid-vapor saturation line in the CO_2-phase diagram. Condensation phenomena in the supersonic gas stream remains an unexplored research topics.For chamber pressure less than 1.85, both rarefication effect and cryogenic effect create physical as well as numerical instability. Our computer experiments to impose an explicit slip wall boundary conditions have failed. The implicit boundary conditions become the necessary step for next trials.

III. FDNS Code Implementation

Currently, the FDNS Code has been comprehensively used for the prediction of the SSME nozzle characteristics in NASA/MSFC[5]. The basic equations employed in the code are the axisymmetric, multi-component conservation equations. A generalized form of these equations written in curvilinear coordinates is given by

$$\frac{1}{J}\frac{\partial(\rho\phi)}{\partial t}=\frac{\partial}{\partial \xi_j}\left(-\rho U_i\phi+\mu_{eff}\,G_{ij}\frac{\partial\phi}{\partial \xi_j}\right)+S_\phi$$

where J, U_i and $G_{i,j}$ represent the Jacobian of the coordinate transformation, contravariant velocities and diffusion metrics respectively.

An unpaid scheme was employed to approximate the convective terms of the momentum, energy and continuity equations. The scheme is based on second and fourth order central differencing with artificial dissipation. First order upwinding is used for the species and turbulence equations, since the parameters involved are positive quantities. Different eigenvalues are used for weighing the dissipation terms depending on the conserved quantity being evaluated, in order to give correct diffusion fluxes near wall boundaries.

For the SSME combuster, the temperature is in the value of 6000°R. It is natural to ask if the wall heat flux includes the radiation contribution. We have added this capability into the FDNS code and delivered it to MSFC ED32, and results were published in ref.[6].

The radiation heat transfer has been hypothesized by a six-flux radiation model, which is based on the Schuster-Hanaker approximation in astrophysical research. For an absorbing-emitting gray medium in local thermodynamic equilibrium, the radiation transport equations describing the variations of the fluxes along six direction can be reduced to the following three second-order ordinary differential equations:

$$\frac{d}{dx}\left(\frac{1}{a+s}\frac{dR_x}{dx}\right)=a(R_x-E)+\frac{S}{3}(2R_x-R_r-R_\theta)$$

$$\frac{1}{r}\frac{d}{dr}\left(\frac{1}{a+s+\frac{1}{r}}\frac{dR_r}{dr}\right)=a(R_r-E)+\frac{S}{3}(2R_r-R_x-R_\theta)$$

$$\frac{1}{r}\frac{d}{d\theta}\left(\frac{1}{a+s}\frac{dR_\theta}{rd\theta}\right)=a(R_\theta-E)+\frac{S}{3}(2R_\theta-R_r-R_x)$$

Where the composite-fluxes R_X, R_Y, and R_θ are defined as :

$$R_x=\frac{1}{2}(I_{x^+}+I_{x^-})$$

$$R_r=\frac{1}{2}(I_{r^+}+I_{r^-})$$

$$R_\theta=\frac{1}{2}(I_{\theta^+}+I_{\theta^-})$$

In these equations, I_X+, I_r+, I_q+, I_X-, I_r- and I_θ^- are the radiation energy fluxes along the positive and negative coordinate directions. The scattering coefficient, s, is defined as the scattering radiation energy per unit length.

The FDNS has been coded and implemented. The calculations have been conducted for the SSME combustor and nozzle. Fig.7 shows the configuration and the computational grid. The grid was generated with more grid point near the wall to predict the large gradient there. Fig.8 shows the isotherm and velocity vector plot of the entire flowfield and Fig.9

shows the averaged radiation flux contours and velocity vector plot. Fig.10 shows the enlarged averaged radiation flux contours in the throat area. Comparisons have been made for the heat flux over the wall and temperature along the centerline with and without radiation contribution. The results are shown in Fig.11 and Fig.12, respectively.

IV. Personnel

In this project, Dr. G. S. Liaw serves as the Principal Investigator to coordinate all the research activities. Dr. J. D. Mo, a Research Assistant Professor, has been working in full time to develop the LU-code since September 15, 1989 until the project was finished.

V. Conclusions

A new computer code for analyzing the axisymmetric nozzle flow with variable gamma has been developed. The validity of this code is demonstrated by the comparisons of present calculations with experimental data. The code has been used to simulate the flowfield in a Carbon Dioxide nozzle having an area ratio of 40. The radiation modeling within the SSME combustor/nozzle has shown that the radiation heat transfer has relatively significant contribution along the nozzle throat, but little effect downstream. The total effect on the wall heat flux is within 5%, which is consistent with the qualitative analysis from MSFC in house results. The code has shown to be efficient and accurate for the flow conditions considered in the present study.

VI. Acknowledgment

The authors are particularly thankful to Dr. Lynn C. Chou (ED33) of NASA/MSFC, who provides all the technical suggestions during the course of this research grant. Dr. Chou's contribution to this research project is incalculable.

VII. Reference

1. Liaw, G. S., "Low Thrust Viscous Nozzle Flow Fields Prediction," Annual Report, 1987.
2. Jameson, A. and Turkel, E., "Implicit Schemes and LU Decompositions," Math. Comp., Vol. 37, No. 156, Oct. 1981.
3. Chou, L. C. and Carter, T. A., "Analytical and Experimental Investigations of a CO_2 Gas Stream Discharging through a Conical Nozzle into a Vacuum Tank," NASA/MSFC Memo. ED33-84-37, July, 1984.
4. Jameson, A. and Yoon, S., "Lowe-Upper Implicit Schemes with Multiple Grids for the Euler Equations," AIAA J., Vol. 25, No. 7, July, 1987.
5. Wang, T.S. and Chen, Y. S., "A Unified Navier-Stokes Flow Field and Performance Analysis of liquid Rocket Engine," AIAA 90-2494
6. Chou, L. C., Wang, T. S., Mo, J. D. and Liaw, G. S., "A Radiation Modeling for the SSME combuster/nozzle Flowfield," The MSFC 9th CFD Working Group Meeting, April 1991
7. MacCormack, R. W., "The effect of Viscosity in Hypervelocity Impact Cratering," AIAA 69-354.
8. Beam, R. M. and Warming, R. F., "An Implicit Finite-Difference Algorithm for Hyperbolic Systems in Conservation-Law Form," J. Comp. Phy. 22, 1976.
9. Steger, J. L. and Warming, R. F., "Flux Vector Splitting of the Inviscid Gasdynamic Equations with Application to Finite-Difference Method," J. Comp. Phy. 40, 1981.

10.Shuen, J. S. and Yoon, S., "Numerical Study of Chemically Reacting Flows Using an LU Scheme," AIAA 88-0436.
11.Yokota, J. W., Caughey, D. A. and Chima, R. V., ' 'A Diagonally Inverted LU Implicit Multigrid Scheme," AIAA 88-3565.
12.Bull, John S., "Precise Attitude Control of the Stanford Relativity Satellite," SUDAAR No. 459, March 1973.
13.Chou, L. C., Liaw, G. S. and Mo, J. D., "Low Thrust Viscous Nozzle Flowfield Predictions," AIAA 91-3436.

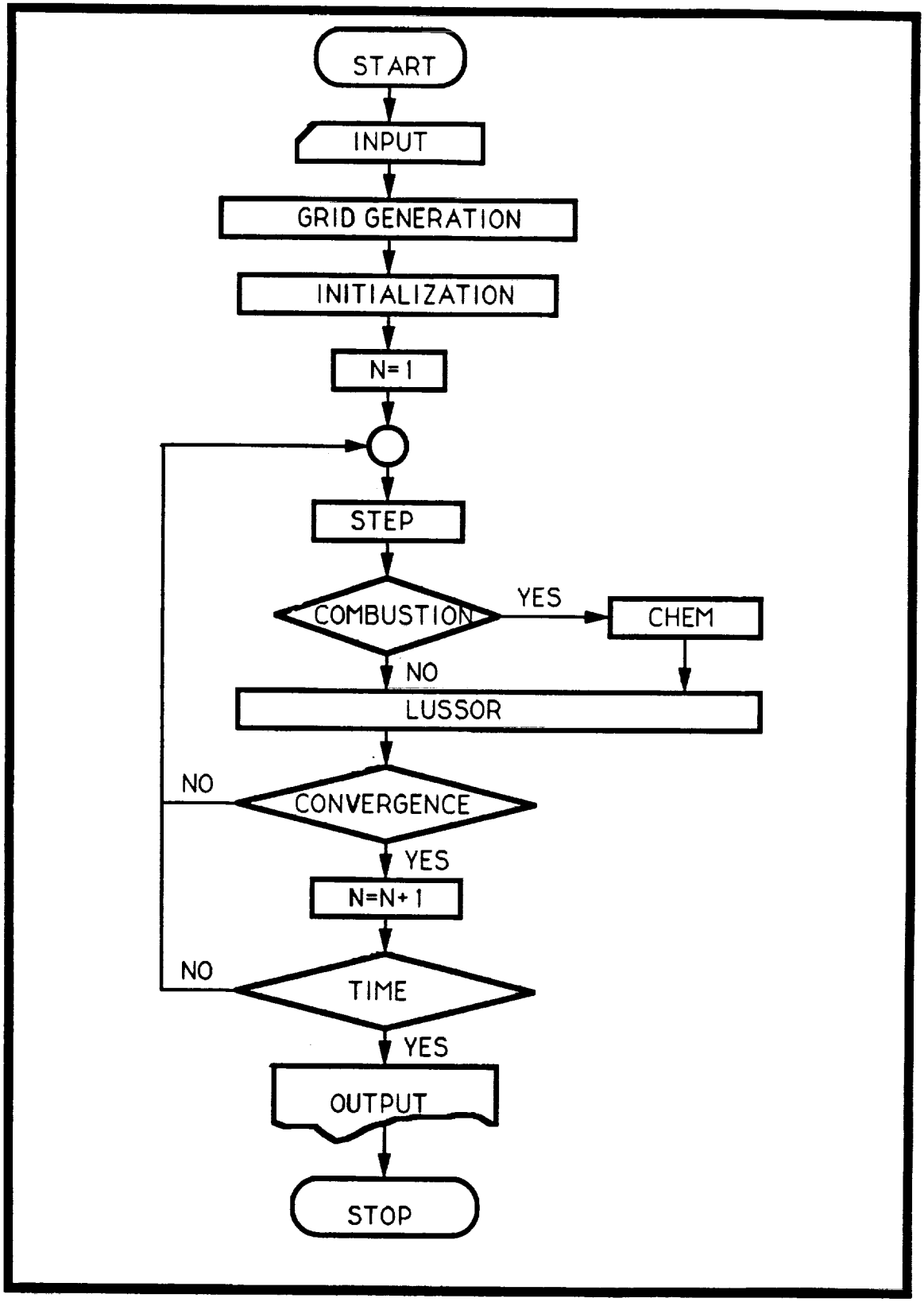

Fig. 2. Flow chart of LU procedure

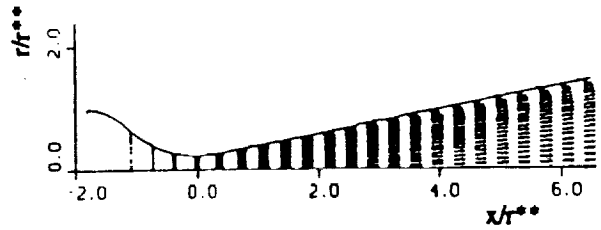

(a) chamber pressure=29.4 psi

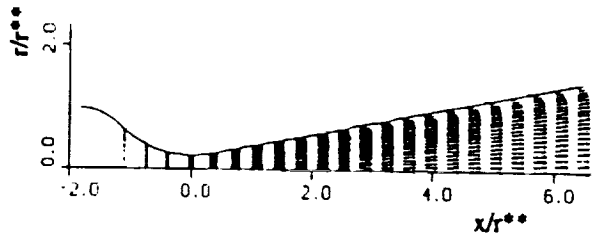

(b) chamber pressure=14.7 psi

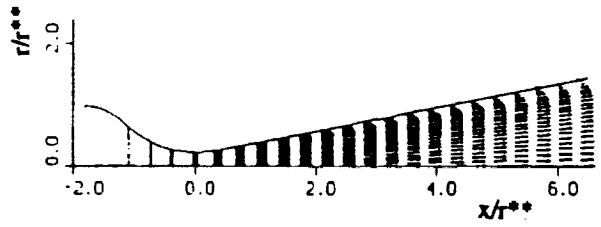

(c) chamber pressure=7.35 psi

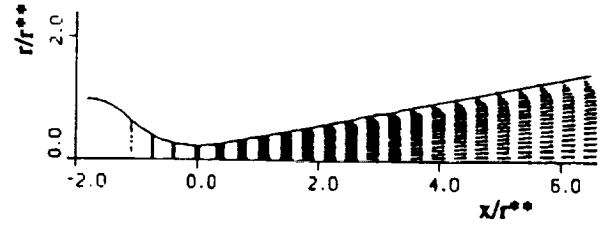

(d) chamber pressure=3.7 psi

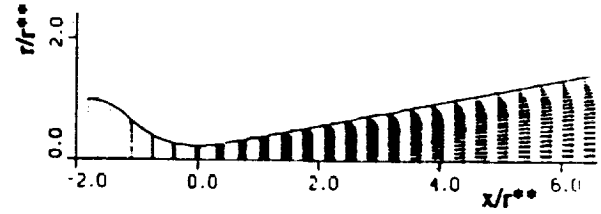

(e) chamber pressure=1.85 psi

Fig. 3. Velocity vector plots at different chamber pressures

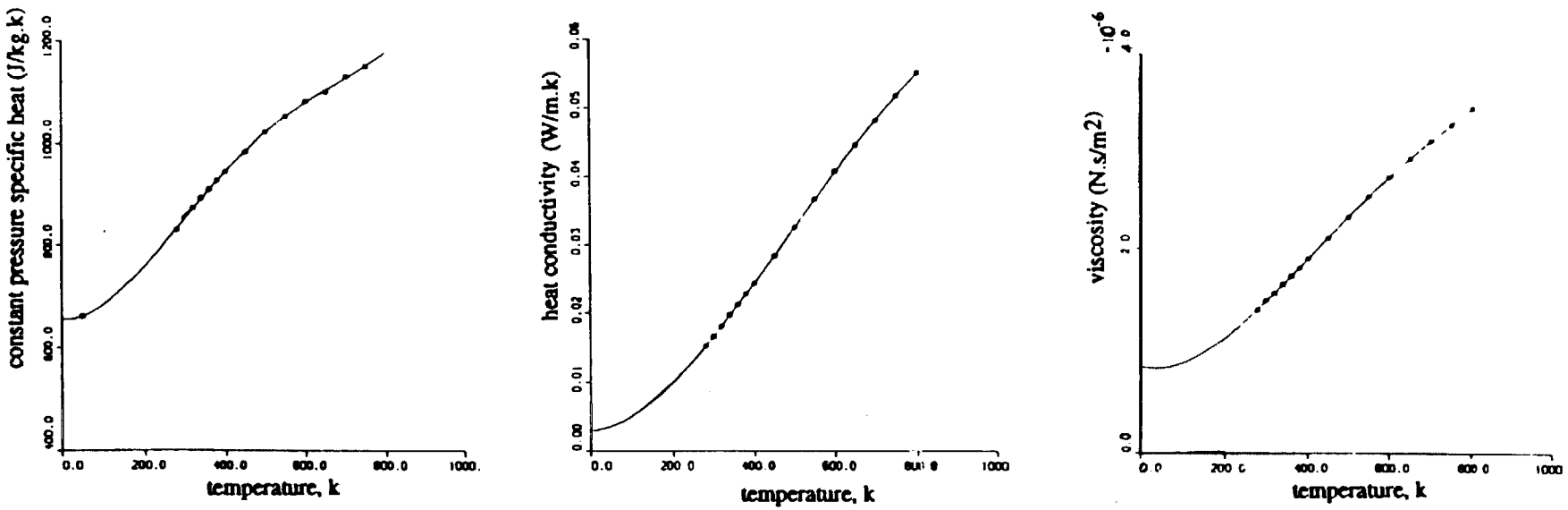

Fig. 4. Variable transport properties of CO_2 and fitted curves

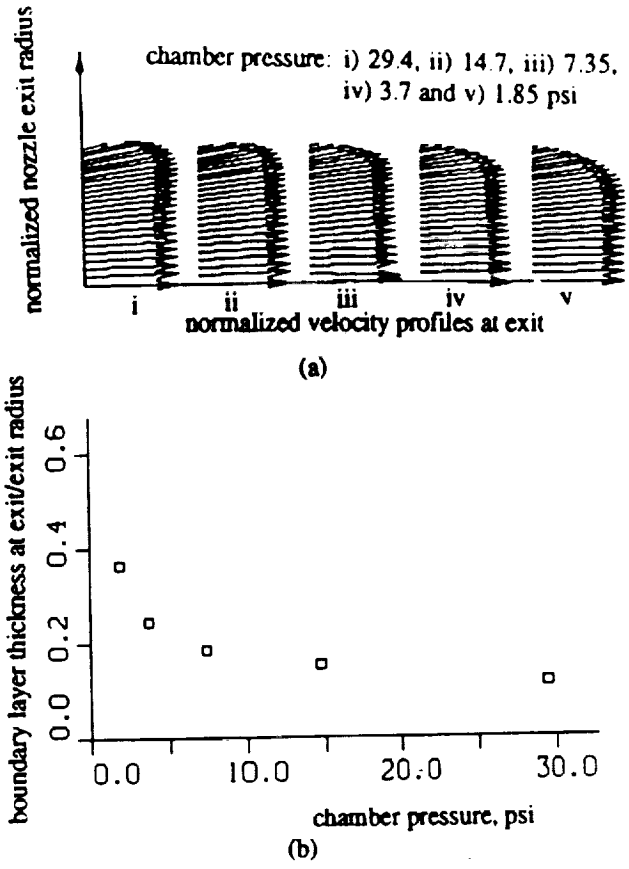

Fig. 5. Velocity profiles and boundary layer thickness at nozzle exit

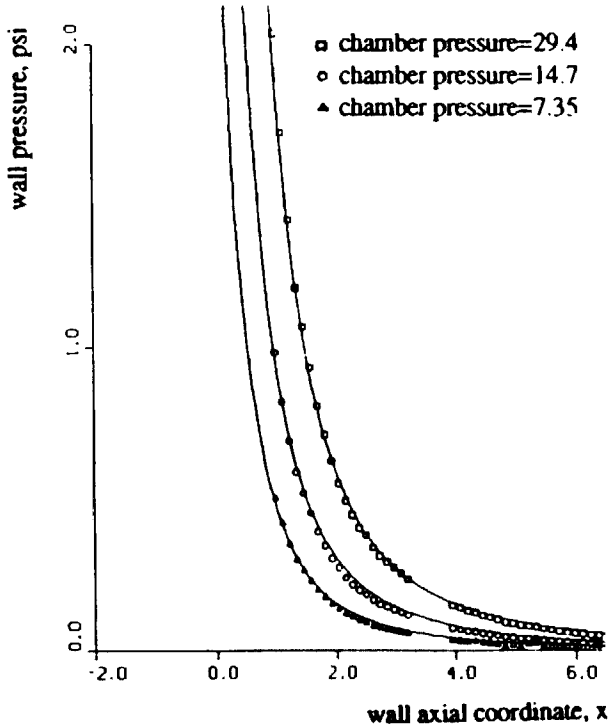

(a) Linear scale

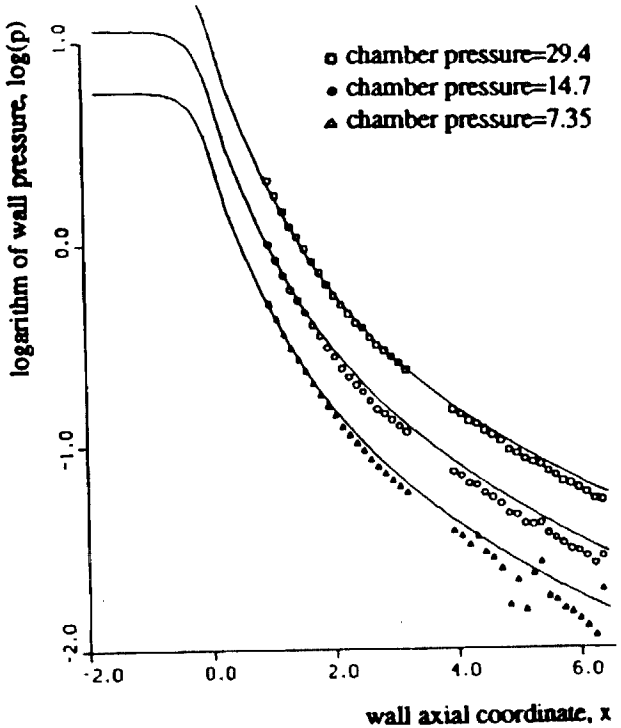

(b) Logarithmic scale

Fig. 6. Comparison of computed wall pressure and test data

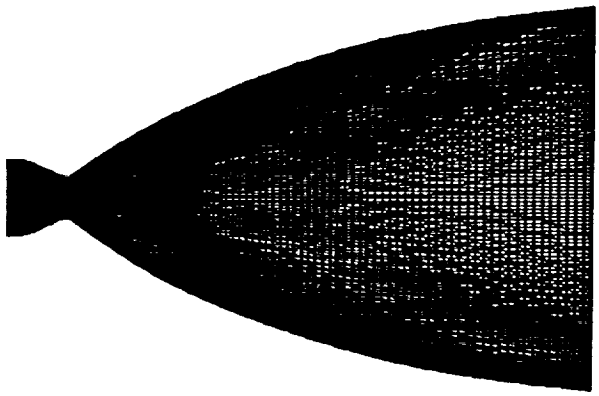

Fig. 7. SSME combustor/nozzle configuration and computational grid

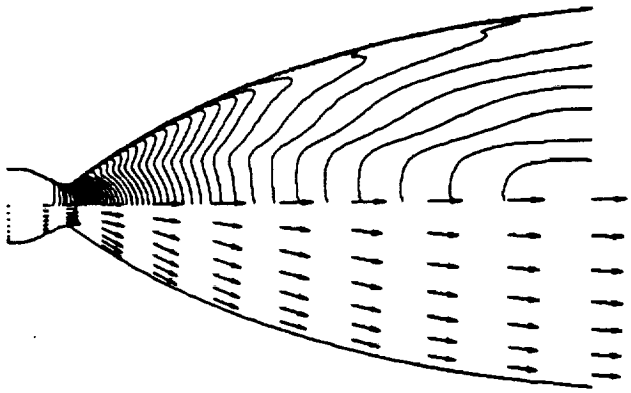

Fig. 8. Isothermal and velocity vector plot of flowfield

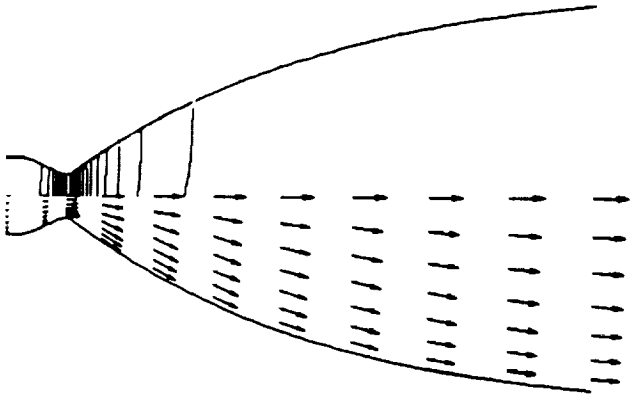

Fig. 9. Averaged radiation flux contours and velocity vector plot

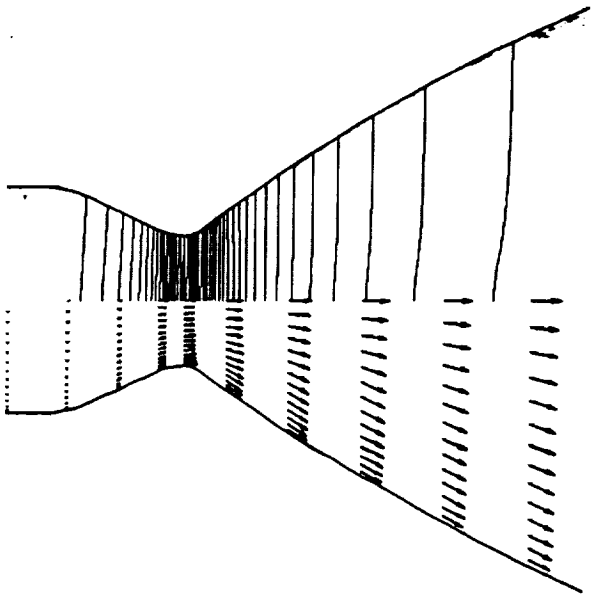

Fig. 10. Enlarged averaged radiation flux contours and velocity vector plot in the throat area

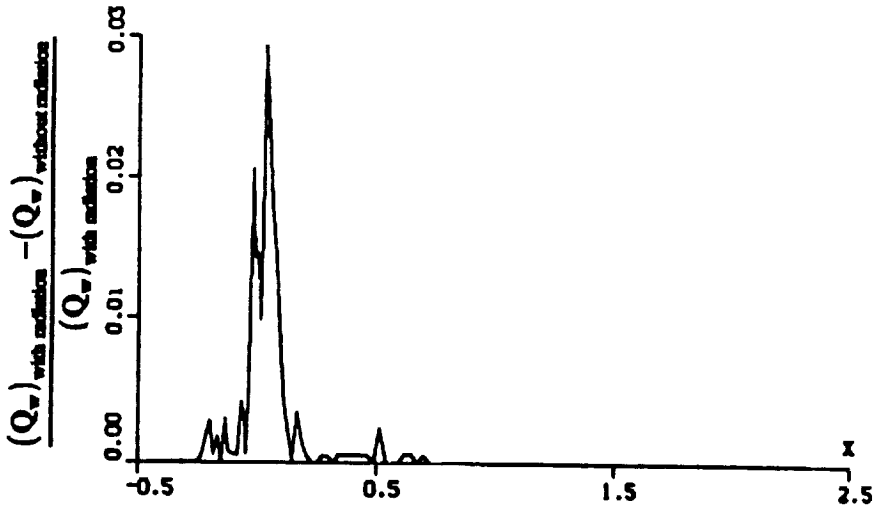

Fig. 11. The relative difference of heat flux over the wall with and without radiation contribution

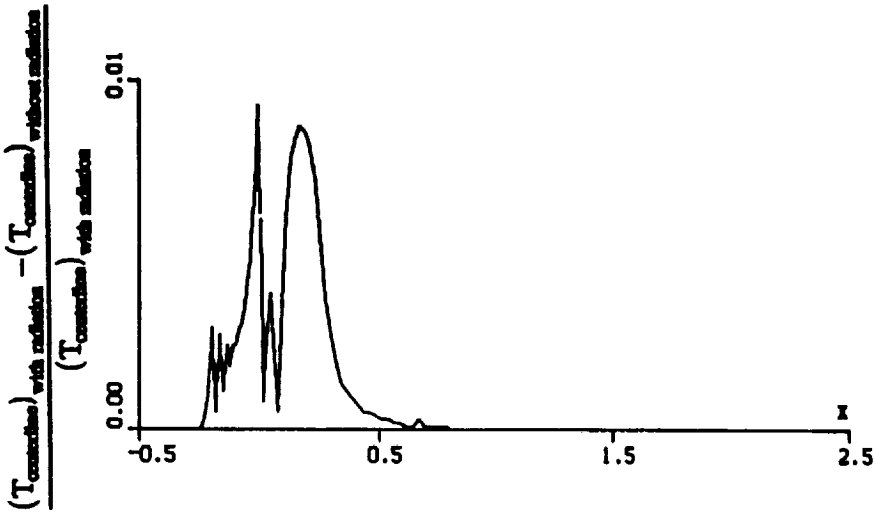

Fig. 12. The relative difference of the temperature along the centerline